RESEARCH ARTICLE | APRIL 26 2024

NH$_3$ adsorption and competition with H$_2$O on a hydroxylated aluminosilicate surface ⊕✓

Giada Franceschi ✉ (iD) ; Andrea Conti (iD) ; Luca Lezuo (iD) ; Rainer Abart (iD) ; Florian Mittendorfer (iD) ;
Michael Schmid (iD) ; Ulrike Diebold (iD)

Check for updates

View Online   Export Citation

NH₃ adsorption and competition with H₂O on a hydroxylated aluminosilicate surface ⓔⓟ

View Online   Export Citation   CrossMark

Giada Franceschi,[1,a] ⓘⒹ Andrea Conti,[1] ⓘⒹ Luca Lezuo,[1] ⓘⒹ Rainer Abart,[2] ⓘⒹ Florian Mittendorfer,[1] ⓘⒹ
Michael Schmid,[1] ⓘⒹ and Ulrike Diebold[1] ⓘⒹ

AFFILIATIONS

[1] Institute of Applied Physics, TU Wien, 1040 Vienna, Austria
[2] Department of Lithospheric Research, Universität Wien, 1090 Vienna, Austria

Note: This paper is part of the 2024 JCP Emerging Investigators Special Collection.
[a] Author to whom correspondence should be addressed: franceschi@iap.tuwien.ac.at

ABSTRACT

The interaction between ammonia (NH_3) and (alumino)silicates is of fundamental and applied importance, yet the specifics of NH_3 adsorption on silicate surfaces remain largely unexplored, mainly because of experimental challenges related to their electrically insulating nature. An example of this knowledge gap is evident in the context of ice nucleation on silicate dust, wherein the role of NH_3 for ice nucleation remains debated. This study explores the fundamentals of the interaction between NH_3 and microcline feldspar ($KAlSi_3O_8$), a common aluminosilicate with outstanding ice nucleation abilities. Atomically resolved non-contact atomic force microscopy, x-ray photoelectron spectroscopy, and density functional theory-based calculations elucidate the adsorption geometry of NH_3 on the lowest-energy surface of microcline, the (001) facet, and its interplay with surface hydroxyls and molecular water. NH_3 and H_2O are found to adsorb molecularly in the same adsorption sites, creating H-bonds with the proximate surface silanol (Si–OH) and aluminol (Al–OH) groups. Despite the closely matched adsorption energies of the two molecules, NH_3 readily yields to replacement by H_2O, challenging the notion that ice nucleation on microcline proceeds via the creation of an ordered H_2O layer atop pre-adsorbed NH_3 molecules.

INTRODUCTION

Ammonia (NH_3) adsorption on solid surfaces is a matter of intense applied and fundamental research. It is integral to environmental and industrial processes such as NH_3 capture for air pollution reduction, NH_3-based fertilizer production, hydrogen storage, and environmental chemistry.[1] Moreover, NH_3 is abundant in space, and its adsorption on interstellar grains is studied to glean insights into the nitrogen chemistry of the interstellar medium, thought to occur predominantly via gas–grain reactions.[2] Fundamentally, NH_3 adsorption processes are regulated by acid–base reactions between different surface sites and NH_3. Because of the exquisite sensitivity of NH_3 adsorption to the local properties of the surface, the adsorption of NH_3 is often used to probe the strength and distribution of surface acidic sites.[3] On oxide surfaces, NH_3 binding can occur in three main ways: via the lone pair of its N atom to a cation that acts as a Lewis acid; by H-bonding via one

of its H atoms to a surface O atom; or by H-bonding via its N atom to an H atom of surface hydroxyl groups (OH). Other feasible ways of ammonia adsorption involve the complete proton transfer from a Brönsted site to create NH_4^+ or NH_3 dissociation into NH_2 (or NH) and OH species.[4]

To ensure a uniform collection of adsorption sites, NH_3 adsorption studies are ideally conducted on atomically controlled single crystals prepared under ultra-high vacuum (UHV). To date, these types of studies have been limited to metals[5–8] and various polymorphs of TiO_2,[9–13] where NH_3 tends to adsorb molecularly on Ti sites via its N lone pair, although dissociation was observed after electron bombardment or on defective surfaces.[9,12] On the other hand, investigations on important materials for NH_3 capture, such as metal-organic frameworks (MOFs) and (alumino)silicates, are typically conducted with porous or amorphous samples.[14–16] In such heterogeneous systems, data interpretation becomes challenging due to surface defects, hydroxyls, or ill-defined atom surroundings that

can affect local acidities.[12,17] In aluminosilicates, further complexity is given by the details of their Si–Al framework: the specific distribution of Al ions can affect the heat of adsorption of NH_3.[16,18] Another important factor is humidity and the water content of the sample; this can affect NH_3 adsorption through cooperative[19] or competitive[20,21] effects between NH_3 and H_2O, potentially leading to NH_3 replacement by H_2O even when the adsorption energy of NH_3 is stronger than that of H_2O.[20] To explore the fundamentals of NH_3 adsorption and its interplay with H_2O on complex systems such as aluminosilicates, well-defined model systems in the form of atomically characterized single crystals investigated under pristine conditions are helpful.

The importance of understanding the details of NH_3 adsorption on aluminosilicates and its interplay with H_2O extends to current atmospheric research on ice nucleation (IN) on mineral dust, an important phenomenon affecting the glaciation of clouds with implications for Earth's climate. K-feldspars, particularly the microcline polymorph ($KAlSi_3O_8$), are crucial IN agents. Microcline's exceptional IN activity[22–29] is generally rationalized through two main perspectives: one emphasizing surface chemistry, which would promote the formation of H-bonded H_2O networks,[30,31] and the other focusing on composition and structural heterogeneities or defects.[32–35] Another important factor is atmospheric chemistry. While traveling in the atmosphere, mineral dust particles are often embedded within aqueous liquid droplets, which can induce preferential dissolution,[36–38] chemical coatings,[39] or net surface charges,[40,41] all of which can impact ice formation. Specifically, it was found that IN activities are substantially enhanced in the presence of dilute NH_3- and NH_4^+-containing solutions.[42–44] However, the underlying reasons are debated. Current interpretations revolve around the replacement of K^+ ions by NH_3 or NH_4^+ as well as their adsorption on the surface, which may offer oriented H bonds for ice growth,[40,42,44,45] and the nature of NH_4^+ ions, which may replace H_2O within the ice network, increasing the configurational entropy of ice and decreasing its overall free energy.[46,47] Experimental investigations on NH_3 adsorption on microcline single crystals and its potential interplay with H_2O may enable testing these hypotheses.

This work explores the fundamentals of the interaction of ammonia with microcline feldspar as a prototypical hydroxylated aluminosilicate. Crystalline microcline samples were cleaved in UHV to expose the lowest-energy (001) surface and investigated by atomically resolved non-contact atomic force microscopy (AFM) and x-ray photoelectron spectroscopy (XPS), complemented by density functional theory (DFT) calculations. By depositing controlled amounts of NH_3 and H_2O molecules at 100 K on microcline (001), it is found that NH_3 adsorbs molecularly by creating H bonds with its surface silanol (Si–OH) and aluminol (Al–OH) groups, occupying the same adsorption site as H_2O with an adsorption energy reaching almost that of H_2O. When H_2O is deposited onto the surface with pre-adsorbed ammonia, it partially replaces the adsorbed NH_3 molecules rather than creating H-bonded networks with the ammonia layer.

MATERIALS AND METHODS

The experiments were carried out in a UHV setup consisting of two interconnected chambers: a preparation chamber for sample cleaving and XPS (base pressure below 1×10^{-10} mbar), and

an adjacent chamber for AFM (1×10^{-11} mbar). A natural microcline feldspar from Russia (from Priv.-Doz. Uwe Kolitsch, Natural History Museum Vienna) was characterized ex situ as detailed elsewhere.[31] (001)-oriented grains from the main crystal were mounted onto Omicron-style stainless-steel sample plates and cleaved in the preparation chamber.[31] After cleaving, the samples exhibited strong surface charges, as was also observed on other cleaved insulators.[48] To remediate such charges, the samples were irradiated for one minute with x rays from the XPS setup.

Water (ultrapure deionized water, MilliQ®, further purified through three freeze–pump–thaw cycles) and anhydrous ammonia (Linde, 99.999%) were dosed from leak valves while keeping the sample holder on the preparation chamber's manipulator at 100 K. The number of molecules deposited is always expressed with respect to the primitive unit cell of the hydroxylated surface (u.c., 0.55 nm^2). The calibration is based on the amount (partial pressure × time) needed to obtain a coverage of 1 molecule/u.c. as judged by AFM, assuming 100% sticking probability. Warming up the sample to room temperature caused the desorption of all H_2O and NH_3 molecules from the hydroxylated surface, as evidenced by XPS and AFM.

XPS was performed with a non-monochromatic dual-anode Mg/Al x-ray source (SPECS XR 50) and a hemispherical analyzer (SPECS PHOIBOS 100). Spectra were acquired in grazing emission (70° from the surface normal). The intensities and positions of the Al-Kα-excited XPS peaks were evaluated with CasaXPS after subtracting a Shirley-type background. For the display and analysis of the XPS data, an energy correction was applied to all spectra to compensate for the charging of the electrically insulating sample. The Si 2p core-level peak was set to 103.10 eV, as reported in the literature.[49] Fitting procedures and parameters are reported in Sec. S3. XPS was used to obtain an approximate desorption temperature for NH_3. A nominal coverage of 5 NH_3 molecules/u.c. was deposited on the UHV-cleaved sample at 100 K. The amount was calibrated based on the dose (pressure × time) needed to observe one NH_3 molecule/u.c. in AFM, assuming a 100% sticking probability. The sample was warmed to increasingly higher temperatures in steps of 10 K, and XPS spectra (N 1s, O 1s, K 2p, and Si 2p for energy correction) were acquired at each stage. The coverage of the molecular NH_3 was roughly halved at a temperature between 150 and 160 K.

The AFM measurements were performed at 4.7 K using a commercial Omicron qPlus low-temperature (LT) head and a differential cryogenic amplifier[50] in constant-height mode. The qPlus AFM sensors (k = 2000–3500 N/m, $f_0 \approx$ 32 kHz, $Q \approx$ 50 000) had a separate contact for the tunneling current. Before each measurement, the tips were prepared on an oxygen-exposed Cu(110) single crystal by repeated indentation and voltage pulses. CuO_x-terminated tips were prepared on the oxygen-induced reconstruction of Cu(110)[51] to exhibit a frequency shift smaller than −1.5 Hz. Local contact potential difference (LCPD) measurements by the Kelvin parabola method[52] were performed to assess residual fields. Residual surface charges were compensated by applying a bias voltage V_s to the back of the sample plate while keeping the tip potential close to the ground.

DFT calculations were performed with the Vienna *Ab initio* Simulation Package (VASP)[53,54] using the r²SCAN-D3 metaGGA exchange-correlation functional.[55] Details about the bulk optimization, unit cell, geometries, cutoff energies, and convergence criteria

are specified elsewhere.[31] The AFM images were simulated with the probe particle model,[56,57] which includes Hartree-potential electrostatics and Lennard-Jones potentials as well as the elastic properties of the tip based on the methods described in Refs. 56 and 57. CuO_x tips were simulated with the following values of lateral and vertical spring constants and charges: $k_{x,y} = 161.9$ N/m, $k_z = 271.1$ N/m, and an effective tip charge of $-0.05e$.[51] The oscillation amplitude for each simulation always matched the one used in the corresponding experimental image. Since the exact height of the tip is not known, simulated AFM images were calculated for different tip heights; the displayed simulated image is the one fitting the experiment best. Tip-sample distances are always referenced to the most protruding surface atom.

RESULTS

Previous studies have shown that microcline (001) readily hydroxylates.[31] Even when the sample was cleaved in UHV, the water entrapped in the mineral and freed during the cleave was sufficient to create a fully hydroxylated layer that was stable at room temperature.[31] Therefore, the starting point of all the experiments in this paper was a hydroxylated surface. As shown in Figs. 1(a) and 1(d), such a layer consists of an ordered array of silanol (Si–OH) and aluminol (Al–OH) groups. When water is dosed below 150 K onto the hydroxylated surface, it adsorbs molecularly at well-defined sites, i.e., in between adjacent silanol and aluminol groups, accepting an H bond from the silanol and donating one to the aluminol.[31] Figures 1(b) and 1(e) show the DFT-optimized models and the experimental AFM images obtained for a coverage of one H_2O molecule per unit cell [in addition to the dissociated H_2O of the hydroxylated surface in Fig. 1(a)]. In experiments performed with CuO_x tips,[51] the appearance of the water species is very sensitive to the tip-sample distance [Figs. S1(a)–S1(d)]. At large distances, H_2O appears with a positive frequency shift (bright); as the tip approaches closer, dark, isolated features suddenly appear. These dark features have a rather sharp boundary and a bright rim, as seen in Fig. 1(b).

Dosing NH_3 below 150 K onto the hydroxylated microcline surface produces a similar structure as the water-exposed one for comparable coverages [Fig. 1(c)]. One dark feature per unit cell is visible, appearing larger and smoother than those caused by H_2O molecules and producing a more gradual frequency change
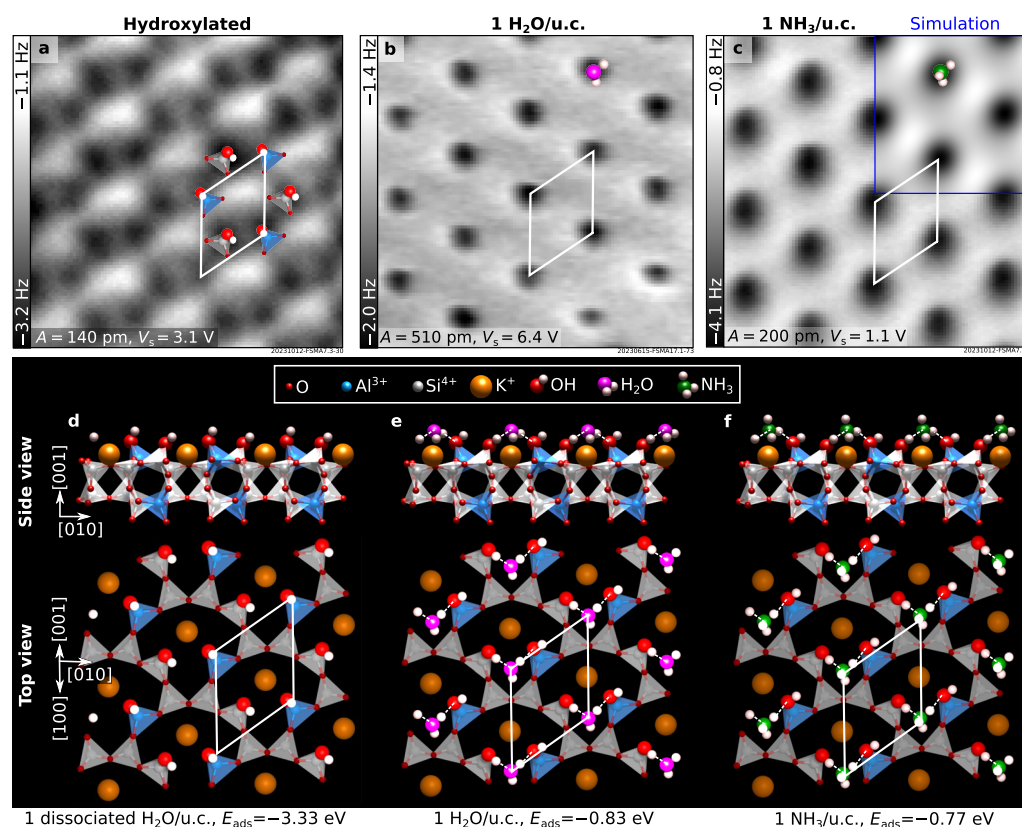
FIG. 1. H_2O and NH_3 adsorption on microcline (001). (a)–(c) 3.2×3.2 nm^2 AFM images of the hydroxylated, H_2O-, and NH_3-exposed microcline (001) surface acquired with CuO_x tips.[51] H_2O and NH_3 were adsorbed at 100 K onto the hydroxylated surface to reach a coverage of one molecule per unit cell (u.c.). (d)–(f) Corresponding DFT models. SiO_4 tetrahedra are gray, and AlO_4 tetrahedra are blue. Panels (d) and (e) are adapted from Ref. 31. The AFM simulation obtained from the model in panel (f) is shown in the inset of panel (c), assuming a tip-sample distance of $d = 5.5$ Å. White rhombi identify primitive unit cells. Calculated adsorption energies (E_{ads}) are reported below the corresponding models.

as a function of the tip-sample distance (for a comparison of images of the NH_3 and H_2O taken with the same tip, see Fig. S1). Figure 1(f) presents the lowest-energy structure found for one adsorbed NH_3 molecule per unit cell. An intact NH_3 occupies the same adsorption site as H_2O. The calculated NH_3 adsorption energy (E_{ads}) is only marginally weaker than for H_2O (-0.77 vs -0.83 eV), consistent with the similar desorption temperature of H_2O and NH_3 (between 150 and 160 K, as inferred from XPS; see Methods). Like H_2O, NH_3 accepts an H bond from a silanol group while donating one to the adjacent aluminol group. One of the two remaining H atoms points away from the surface; the other one lies within the surface and points in the same direction as the free H atom of adsorbed H_2O. The corresponding AFM simulation, superimposed on the experimental image of Fig. 1(c), reproduces the experimental contrast.

In XPS, the N 1s peak measured on a surface covered by 1 NH_3/u.c. sits at 400.4 eV XPS binding energy after correction for charging[31] (see Sec. S3 for details). The peak intensity increases with ammonia deposition at 100 K while preserving its position and width until the nominal amount of ≈ 4 NH_3/u.c., after which the intensity saturates (see Sec. S3). This suggests that multilayer adsorption is possible only below 100 K, consistent with previous temperature programmed desorption studies on crystalline forsterite (Mg_2SiO_4)[2] and TiO_2,[13] which observed the multilayer NH_3 desorption peak around 100 K. Warming up the NH_3-covered sample to room temperature causes the intensity to decrease and leads to the eventual disappearance of the N 1s peak without the formation of any shoulders, suggesting that NH_3 desorbs from the surface as an intact molecule.

To test whether adsorbed NH_3 can serve as a template for an ordered and oriented layer of water ice, H_2O was deposited at 100 K on the NH_3-saturated surface of Figs. 1(c) and 1(f). In XPS [Fig. 2(a)], the H_2O component of the O 1s peak (black) increases as a function of the H_2O coverage, as expected. However, the increase is significantly smaller than when H_2O is deposited directly on the hydroxylated surface (gray), indicating that fewer H_2O molecules stick to the surface with pre-adsorbed NH_3. (While this could also indicate that 3D clusters are formed, which contribute less to the XPS intensity, the AFM data discard this hypothesis.) At the same time, the N 1s signal (green) decreases. Figures 2(b)–2(d) show the evolution of selected N 1s and the O 1s peaks (see Sec. S3 for details about the fitting procedures).

The AFM images in Fig. 3 help interpreting the XPS trends. Dosing a nominal amount of 2.5 H_2O/u.c. onto the surface with pre-adsorbed NH_3 produces the surface shown in Fig. 3(a). Most of it appears as light-gray areas with weak modulations of Δf. When imaged at closer tip-sample distances [Fig. 3(d)], these areas have the same appearance as the hydroxylated surface with a mixture of H_2O and NH_3 molecules [compare with Figs. 1(b) and 1(c)]. Similar to the case of single-molecule adsorption, it is evident that in the mixed phase, the H_2O and NH_3 molecules occupy the same site as the unit cell. The deposited H_2O has substituted $\approx 40\%$ of the pre-adsorbed NH_3 molecules. In addition to the areas of coexisting NH_3 and H_2O, a few isolated darker dots are visible in Fig. 3(a). Darker contrast indicates a stronger, more attractive interaction with the AFM tip during constant-height image acquisition. It is attributed to water species deposited on top of the mixture of NH_3 and H_2O, thus sticking out further from the surface. In the top part of Fig. 3(a),
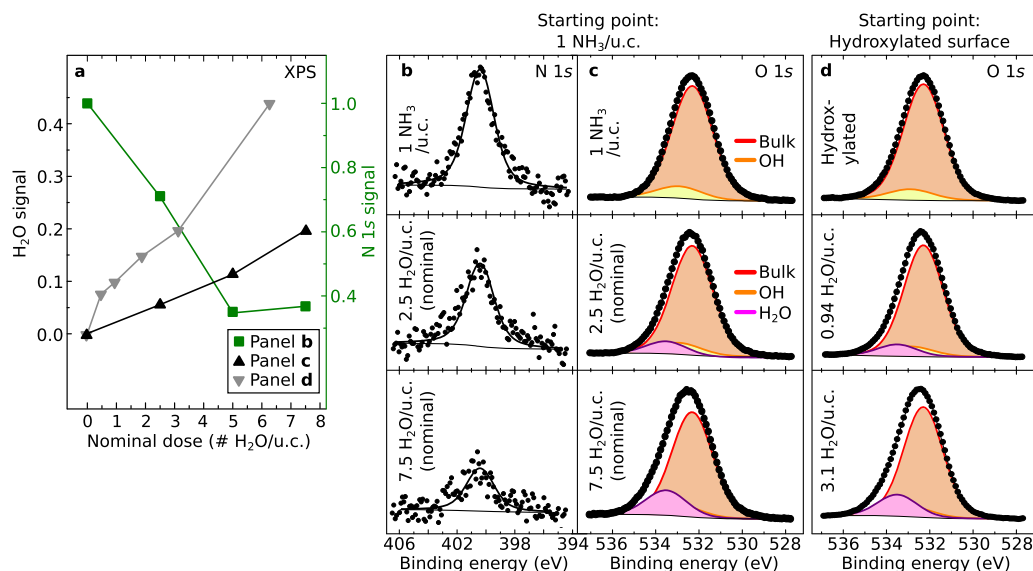

FIG. 2. Substitution of NH_3 by H_2O measured with XPS. (a) XPS signals as a function of nominal H_2O dose for adsorption at 100 K onto an NH_3-exposed surface (green, squares: N 1s; black, upward-pointing triangles: H_2O component of O 1s) and over a hydroxylated surface without NH_3 (gray, downward-pointing triangles: H_2O component of O 1s). N 1s counts are normalized to the peak area obtained for 1 NH_3/u.c.; H_2O areas are normalized to the O 1s bulk component of the O 1s peak before any H_2O exposure. Error bars on the intensities are comparable to the symbol sizes. The nominal doses do not account for intrinsic errors due to pumping by the chamber walls. Lines connecting symbols are meant to guide the eye. (b)–(d) Evolution of selected N 1s and O 1s spectra with corresponding fits. Nominal H_2O doses are noted at the sides of the corresponding panels. For all spectra: Al Kα, 1486.61 eV, pass energy 20 eV, 70° grazing emission. Binding energy axes were adjusted to account for charging (see Methods). The O 1s peak was fit as described in Sec. S3.
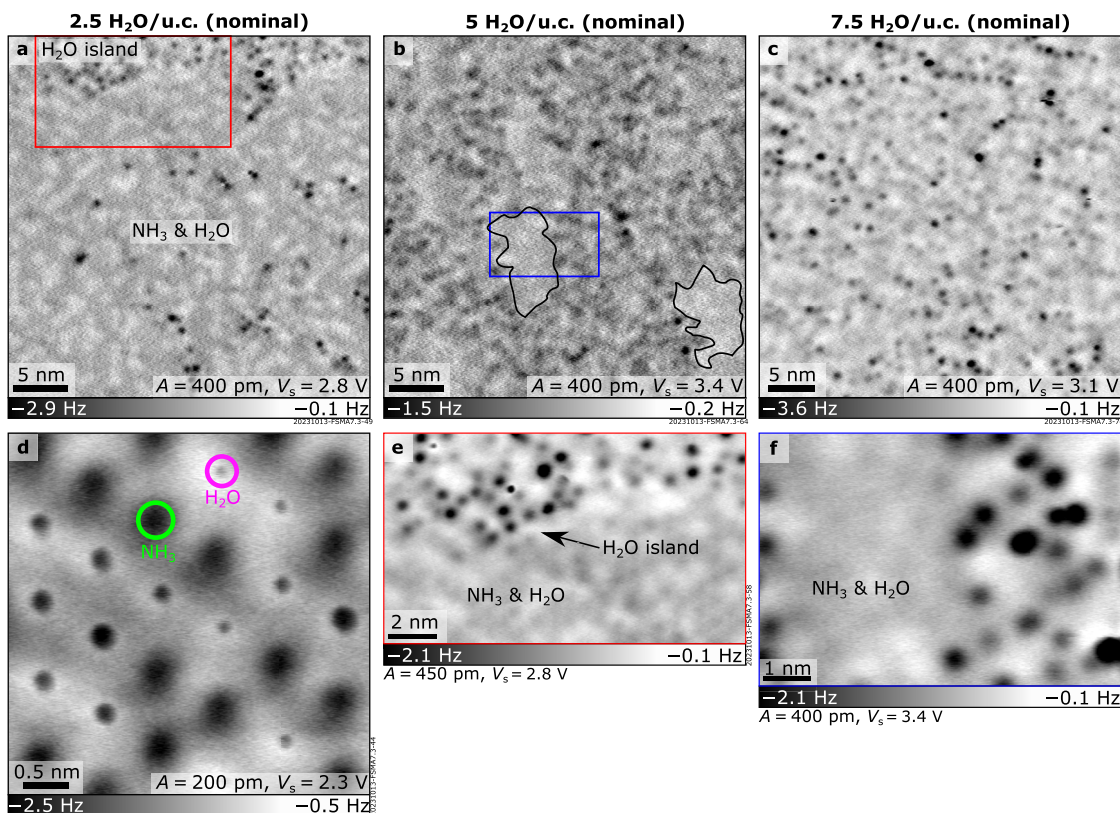
FIG. 3. Substitution of NH_3 by H_2O, AFM. (a)–(f) AFM images of a surface exposed to NH_3 at 100 K [gas dose corresponding to 1 molecule per unit cell, as in Figs. 1(c) and 1(f)], followed by H_2O exposure. (a), (d), (e) Nominal gas dose of 2.5 H_2O/u.c. (a) The majority of the surface appears as a mixture of H_2O and NH_3, as seen in more detail in panel (d). The top portion of panel (a), imaged at a closer tip-sample distance in panel (e), evidences the growth of additional H_2O. (b), (f) Nominal gas dose of 5 H_2O/u.c.: The surface is almost fully covered by H_2O islands. Small patches remain in which adsorbed H_2O and NH_3 coexist, two of which are marked by dark outlines. The area marked by the blue rectangle is imaged at a closer tip-sample distance in panel (f). (c) Nominal gas dose of 7.5 H_2O/u.c.: The surface is fully covered by a disordered H_2O layer.

imaged at a closer tip-sample distance in Fig. 3(e), a cluster of such darker features is visible. This cluster resembles what is observed by dosing H_2O directly onto the hydroxylated surface without any pre-adsorbed NH_3 (Sec. S2). However, in the absence of pre-adsorbed NH_3, the water islands are significantly larger for comparable gas doses, consistent with the higher H_2O signals measured in XPS [Fig. 2(a)]. Additionally, the water islands resulting from deposited water only display internal short-range ordering; such ordering is absent in the water islands of Fig. 3.

The water islands grow bigger with increasing water coverages [see Figs. 3(b) and 3(c)], where the nominal gas doses correspond to 5 H_2O and 7.5 H_2O/u.c., respectively. In Fig. 3(b), the water islands occupy almost the whole surface (the dark dots are not as well resolved as in Fig. 3(a) because the image is acquired with the tip further away from the surface). A few small, bright patches remain where H_2O and NH_3 coexist; two of these areas are marked. In Fig. 3(c), the surface is fully covered by the protruding water islands; several dark spots with different attractive contrasts and without any long-range ordering are visible. In XPS [Fig. 2(a)], the NH_3 signal has already reached its minimum at the nominal gas dose of 5 H_2O/u.c., indicating that H_2O replaces NH_3 only to a certain extent.

Therefore, H_2O grows atop the mixed layer of NH_3 and H_2O. Note that it cannot be excluded that a small fraction of NH_3 molecules participate into the growth of the water islands mentioned earlier.

DISCUSSION

Molecular insights into NH₃ adsorption

The (001) surface investigated here is the lowest-energy facet of microcline. Therefore, it is likely that this is a common surface termination also for mineral dust particles. It serves as a model system to investigate the adsorption mechanisms of gas-phase ammonia and water on hydroxylated aluminosilicate surfaces. The data reveal that NH_3 deposited below 150 K adsorbs molecularly via H bonds with the available surface hydroxyls. It is reasonable for molecular adsorption to prevail over the formation of NH_4^+ ions or NH_3 dissociation upon adsorption. The strong energy gain associated with surface hydroxylation [adsorption energy of ≈ -3.3 eV/H_2O, see Fig. 1(b)[31]] outweighs the interaction between NH_3 and the hydroxyl groups [adsorption energy of ≈ -0.8 eV, see Fig. 1(c)], making the transfer

of protons from silanols to NH$_3$ to create NH$_4^+$ unlikely. The situation could be different in solution, however, where the ready availability of protons may stabilize NH$_4^+$ ions while maintaining the surface hydroxyls. NH$_3$ dissociation is also not expected because of the lack of available surface O sites that would accept a proton.

The NH$_3$ molecule acts as both an H-bond acceptor and an H-bond donor in the adsorption configuration on microcline. According to the general expectation, NH$_3$ should accept H bonds from surface OH groups by forming an H bond between its N atom and the H atom of the OH group.[4,21] Because of the favorable geometry of surface hydroxyls on the hydroxylated microcline surface, NH$_3$ here exhibits amphoteric behavior with respect to H bonds: The NH$_3$ molecule engages with two proximate OH groups by accepting an H-bond from the silanol and donating one to the aluminol. The individual behaviors of silanols (H-bond donating) and aluminols (H-bond accepting) are determined by their coordination chemistry. The larger charge of silicon compared to aluminum (oxidation state +4 vs +3) strengthens the Si–OH bond relative to the Al–OH bond, making it easier to release H from Si–OH than from Al–OH. These considerations equally apply to the adsorption of H$_2$O, which occupies the same site as NH$_3$ and interacts with proximate OH groups in a similar manner.[31]

The results demonstrate the significance of the atomic environment in determining the acidity of surface hydroxyls, as already predicted by previous computational studies on amorphous silica, where variations in the exact coordination and atomic environment lead to distinct acid behaviors even for the same hydroxyl type.[15,17,58] Extending these reasonings to aluminosilicates, one expects that the relative density and distribution of aluminol and silanol groups (and thus, of Si and Al ions in the Si–Al framework) will affect local acidities. Consistently, zeolites and mesoporous silica evidence changes in heats of adsorption for NH$_3$ and acidity in response to alterations in Al concentrations and distributions.[16,18,59] Therefore, accurate acidity measurements on aluminosilicate surfaces necessitate careful consideration of the distribution and geometric proximity of aluminols and silanols. In this respect, other terminations of microcline besides the (001) surface investigated here, as well as other polymorphs exposing surfaces with different arrangements of silanol and aluminol groups, are expected to produce adsorption configurations of ammonia and water differing from those reported here.

Interplay between NH$_3$ and H$_2$O and implications for atmospheric ice nucleation

Figures 2 and 3 illustrate how a hydroxylated surface pre-dosed with NH$_3$ changes after exposure to H$_2$O at low temperatures. H$_2$O does not simply adsorb atop NH$_3$. Instead, it tends to substitute adsorbed NH$_3$, as judged by the coexistence of H$_2$O and NH$_3$ at equivalent adsorption sites seen in Figs. 3(a) and 3(d) and by the XPS trends of Fig. 2(a). For comparable H$_2$O doses, the H$_2$O signals are larger for the hydroxylated surface without NH$_3$ compared to the NH$_3$-pre-adsorbed one, suggesting that H$_2$O sticks less to the latter. Such sticking effects are likely due to the competition of H$_2$O and NH$_3$ to adsorb on the same site, which promotes the substitution of the adsorbed species over H$_2$O growth atop NH$_3$. A chemical interaction of H$_2$O with NH$_3$ is deemed unlikely. If one of the H atoms of H$_2$O were to interact with NH$_3$ to transform it, e.g., to NH$_4^+$, a shift of $\approx$2 eV in the N 1s peak would be expected,[60] which is not

present here. Moreover, an attractive interaction between H$_2$O and NH$_3$ would favor NH$_3$ to remain on the surface. On the contrary, the N 1s signal decreases with increasing H$_2$O dose. This indicates that NH$_3$ and H$_2$O compete for adsorption sites and speaks against a strong binding between them.

Notably, the substitution occurs despite the minimal energy differences in the adsorption energies of H$_2$O and NH$_3$ predicted by DFT (-0.83 vs -0.77 eV). Similar effects have been previously observed within MOF cages,[20] where NH$_3$ molecules bound to metal centers can be readily substituted by H$_2$O even when NH$_3$ has significantly stronger adsorption energies. This behavior was attributed to cooperative effects between the H$_2$O molecules as well as a strong interaction between H$_2$O and NH$_3$, which can weaken the bond between NH$_3$ and the metal center while reducing the kinetic barriers to perform the substitution. Similarly, incoming H$_2$O molecules onto the microcline surface with pre-adsorbed NH$_3$ may interact with the adsorbed NH$_3$ via H-bonding, weakening the bond between NH$_3$ and the surface OH and eventually leading to its detachment. After $\approx$40% of NH$_3$ has been substituted by H$_2$O, H$_2$O islands grow atop the mixed NH$_3$–H$_2$O layer.

The current investigation contributes to ongoing discussions on atmospheric IN on microcline and the role of ammonia in this process. The mechanisms leading to enhanced IN activities of microcline upon immersion in ammonia solutions[42–44] are currently debated. Some studies emphasize the role of the direct adsorption of NH$_3$ or NH$_4^+$ to the surface hydroxyls.[42] In this case, the oriented, extra protons offered by the adsorbed NH$_3$ molecules should favor the formation of ordered H-bonded networks and thus facilitate IN.[40,42,45] This picture is supported by sum frequency generation studies on silica surfaces, indicating that adsorbed NH$_3$ enforces a net orientation of H$_2$O molecules at the ice-silica interface.[45] The present study shows that, during gas–phase interaction under UHV conditions, H$_2$O does not orderly bind on top of a layer of adsorbed NH$_3$. Instead, the two species compete for the same adsorption sites, leading to a partial replacement of NH$_3$ by H$_2$O. In the atmosphere, NH$_3$ has a drastically lower concentration than H$_2$O, existing in parts per billion. Under the oversimplified assumption of gas–phase interactions between microcline and the two substances in the atmosphere, one expects H$_2$O adsorption to prevail over NH$_3$ because of the concentration differences between the two species and their comparable binding energies. Therefore, in this context, the mere adsorption of water over ammonia can be ruled out as a dominant factor for increased IN activities. However, the situation will be different in liquid and thick ice layers. Effects proposed in the literature, such as pH-dependent surface charge, ion exchange (K$^+$ for NH$_4^+$),[44] or preferential dissolution, may dominate. Moreover, some studies suggest that the effect of ammonia solutions is related to the peculiar properties of the NH$_4^+$ ions: NH$_4^+$ is prone to replace H$_2$O within the ice network while offering an additional proton for H bonding, increasing the configurational entropy of the ice structure and thus lowering its free energy.[46,47]

CONCLUSIONS

This work sheds light on the molecular-scale interaction of gaseous NH$_3$ with a prototypical aluminosilicate, particularly one prone to hydroxylation upon exposure to water vapor. Based on the phase diagram in Ref. 31, the surface of microcline (001) should

26 April 2024 10:01:41

be hydroxylated [as in Fig. 1(a)] under ambient conditions as well. The stability of the hydroxylated surface makes it pertinent for fundamental investigations of environmental processes such as atmospheric ice nucleation. Through atomically resolved AFM imaging and DFT-based calculations, it was found that NH_3 adsorbs molecularly on hydroxylated microcline feldspar (001) by H-bonding to its surface aluminol and silanol groups. The geometric proximity and coordination chemistry of the two hydroxyl groups determine the specific adsorption configuration of NH_3, which acts as both an H-bond donor and an H-bond acceptor. The intimate link between the adsorption geometry of NH_3 and the type and distribution of surface OH groups evidenced here stresses the importance of determining the distribution of surface Si and Al tetrahedra for reliable acidity measurements of aluminosilicates. When water is introduced onto the surface with pre-adsorbed NH_3, it competes for the same adsorption sites, leading to partial replacement and precluding the growth of ordered water networks over adsorbed NH_3.

SUPPLEMENTARY MATERIAL

Section S1: AFM images at different tip-sample distances. Section S2: Dosing H_2O directly on the hydroxylated surface. Section S3: XPS spectra.

ACKNOWLEDGMENTS

AUTHOR DECLARATIONS

Conflict of Interest

The authors have no conflicts to disclose.

Author Contributions

Giada Franceschi: Conceptualization (equal); Formal analysis (equal); Investigation (equal); Supervision (equal); Writing – original draft (equal); Writing – review & editing (equal). **Andrea Conti**: Formal analysis (equal); Investigation (equal); Writing – review & editing (equal). **Luca Lezuo**: Writing – review & editing (equal). **Rainer Abart**: Validation (equal); Writing – review & editing (equal). **Florian Mittendorfer**: Supervision (equal); Writing – review & editing (equal). **Michael Schmid**: Validation (equal); Writing – review & editing (equal). **Ulrike Diebold**: Conceptualization (equal); Funding acquisition (equal); Supervision (equal); Validation (equal); Writing – review & editing (equal).

DATA AVAILABILITY

The data that support the findings of this study are available from the corresponding author upon reasonable request.

REFERENCES

[1] B. Han, C. Butterly, W. Zhang, J. Z. He, and D. Chen, "Adsorbent materials for ammonium and ammonia removal: A review," J. Cleaner Prod. **283**, 124611 (2021).

[2] T. Suhasaria, J. D. Thrower, and H. Zacharias, "Thermal desorption of ammonia from crystalline forsterite surfaces," Mon. Not. R. Astron. Soc. **454**(3), 3317–3327 (2015).

[3] A. Gervasini and A. Auroux, "Microcalorimetric investigation of the acidity and basicity of metal oxides," J. Therm. Anal. **37**(8), 1737–1744 (1991).

[4] A. A. Tsyganenko, D. V. Pozdnyakov, and V. N. Filimonov, "Infrared study of surface species arising from ammonia adsorption on oxide surfaces," J. Mol. Struct. **29**(2), 299–318 (1975).

[5] C. Klauber, M. D. Alvey, and J. T. Yates, "NH_3 adsorption on Ni(110) and the production of the NH_2 species by electron irradiation," Surf. Sci. **154**(1), 139–167 (1985).

[6] T. E. Madey and C. Benndorf, "Influence of surface additives (Na and O) on the adsorption and structure of NH_3, on Ni(110)," Surf. Sci. **153**, 587–595 (1985).

[7] B. D. Kay, K. R. Lykke, J. R. Creighton, and S. J. Ward, "The influence of adsorbate–absorbate hydrogen bonding in molecular chemisorption: NH_3, HF, and H_2O on Au(111)," J. Chem. Phys. **91**(8), 5120–5121 (1989).

[8] C. Xu and D. W. Goodman, "Adsorption of ammonia and its influence on coadsorbed carbon monoxide on monolayer and multilayer palladium epitaxially grown on Mo(110)," J. Phys. Chem. B **102**(22), 4392–4400 (1998).

[9] U. Diebold and T. E. Madey, "Adsorption and electron stimulated desorption of NH_3/TiO_2(110)," J. Vac. Sci. Technol., A **10**(4), 2327–2335 (1992).

[10] S. Koust, K. C. Adamsen, E. L. Kolsbjerg, Z. Li, B. Hammer, S. Wendt, and J. V. Lauritsen, "NH_3 adsorption on anatase-TiO_2(101)," J. Chem. Phys. **148**, 124704 (2018).

[11] J. N. Wilson and H. Idriss, "Reactions of ammonia on stoichiometric and reduced TiO_2(001) single crystal surfaces," Langmuir **20**(25), 10956–10961 (2004).

[12] H. Bühlmeyer, K. C. Adamsen, T. Xu, L. Lammich, J. Libuda, J. V. Lauritsen, and S. Wendt, "Adsorption and reaction of NH_3 on rutile TiO_2(110): An STM study," J. Phys. Chem. C **126**(15), 6590–6600 (2022).

[13] B. Kim, Z. Li, B. D. Kay, Z. Dohnálek, and Y. K. Kim, "The effect of oxygen vacancies on the binding interactions of NH_3 with rutile TiO_2(110)-1 × 1," Phys. Chem. Chem. Phys. **14**(43), 15060–15065 (2012).

[14] G. A. Blomfield and L. H. Little, "Chemisorption of ammonia on silica," Can. J. Chem. **51**, 1771–1781 (1973).

[15] A. M. Jystad, A. Biancardi, and M. Caricato, "Simulations of ammonia adsorption for the characterization of acid sites in metal-doped amorphous silicates," J. Phys. Chem. C **121**(40), 22258–22267 (2017).

[16] G. I. Kapustin, T. R. Brueva, A. L. Klyachko, S. Beran, and B. Wichterlova, "Determination of the number and acid strength of acid sites in zeolites by ammonia adsorption," Appl. Catal. **42**(2), 239–246 (1988).

[17] M. Pfeiffer-Laplaud, D. Costa, F. Tielens, M. P. Gaigeot, and M. Sulpizi, "Bimodal acidity at the amorphous silica/water interface," J. Phys. Chem. C **119**(49), 27354–27362 (2015).

[18] B. Zhakisheva, J. J. Gutiérrez-Sevillano, and S. Calero, "Ammonia and water in zeolites: Effect of aluminum distribution on the heat of adsorption," Sep. Purif. Technol. **306**, 122564 (2023).

[19] N. Nijem, K. Fürsich, H. Bluhm, S. R. Leone, and M. K. Gilles, "Ammonia adsorption and Co-adsorption with water in HKUST-1: Spectroscopic evidence for cooperative interactions," J. Phys. Chem. C **119**(44), 24781–24788 (2015).

[20] K. Tan, S. Ullah, H. Pandey, E. M. Cedeño-Morales, H. Wang, K. Wang, H. C. Zhou, J. Li, and T. Thonhauser, "Competitive adsorption of NH_3 and H_2O in metal-organic framework materials: MOF-74," Chem. Mater. **34**, 7906 (2022).

[21] D. W. James and M. E. Harward, "Competition of NH_3 and H_2O for adsorption sites on clay minerals," Soil Sci. Soc. Am. J. **28**(5), 636–640 (1964).

[22] J. D. Atkinson, B. J. Murray, M. T. Woodhouse, T. F. Whale, K. J. Baustian, K. S. Carslaw, S. Dobbie, D. O'Sullivan, and T. L. Malkin, "The importance of feldspar for ice nucleation by mineral dust in mixed-phase clouds," Nature **498**(7454), 355–358 (2013).

[23] A. D. Harrison, T. F. Whale, M. A. Carpenter, M. A. Holden, L. Neve, D. O'Sullivan, J. Vergara Temprado, and B. J. Murray, "Not all feldspars are equal: A

survey of ice nucleating propertiesacross the feldspar group of minerals," Atmos. Chem. Phys. **16**(17), 10927–10940 (2016).

[24] J. D. Yakobi-Hancock, L. A. Ladino, and J. P. D. Abbatt, "Feldspar minerals as efficient deposition ice nuclei," Atmos. Chem. Phys. **13**(22), 11175–11185 (2013).

[25] T. Zolles, J. Burkart, T. Häusler, B. Pummer, R. Hitzenberger, and H. Grothe, "Identification of ice nucleation active sites on feldspar dust particles," J. Phys. Chem. A **119**(11), 2692–2700 (2015).

[26] A. Welti, U. Lohmann, and Z. A. Kanji, "Ice nucleation properties of K-feldspar polymorphs and plagioclase feldspars," Atmos. Chem. Phys. **19**(16), 10901–10918 (2019).

[27] M. A. Holden, J. M. Campbell, F. C. Meldrum, B. J. Murray, and H. K. Christenson, "Active sites for ice nucleation differ depending on nucleation mode," Proc. Natl. Acad. Sci. U. S. A. **118**(18), 1–9 (2021).

[28] L. Kaufmann, C. Marcolli, J. Hofer, V. Pinti, C. R. Hoyle, and T. Peter, "Ice nucleation efficiency of natural dust samples in the immersion mode," Atmos. Chem. Phys. **16**(17), 11177–11206 (2016).

[29] M. J. Pankhurst, "Atmospheric K-feldspar as a potential climate modulating agent through geologic time," Geology **45**(4), 379–382 (2017).

[30] M. A. Freedman, "Potential sites for ice nucleation on aluminosilicate clay minerals and related materials," J. Phys. Chem. Lett. **6**, 3850–3858 (2015).

[31] G. Franceschi, A. Conti, L. Lezuo, R. Abart, F. Mittendorfer, M. Schmid, and U. Diebold, "How water binds to microcline feldspar (001)," J. Phys. Chem. Lett. **15**(1), 15–22 (2024).

[32] T. F. Whale, M. A. Holden, A. N. Kulak, Y. Y. Kim, F. C. Meldrum, H. K. Christenson, and B. J. Murray, "The role of phase separation and related topography in the exceptional ice-nucleating ability of alkali feldspars," Phys. Chem. Chem. Phys. **19**(46), 31186–31193 (2017).

[33] A. Kiselev, A. Keinert, T. Gaedeke, T. Leisner, C. Sutter, E. Petrishcheva, and R. Abart, "Effect of chemically induced fracturing on the ice nucleation activity of alkali feldspar," Atmos. Chem. Phys. **21**, 11801–11814 (2021).

[34] M. A. Holden, T. F. Whale, M. D. Tarn, D. O'Sullivan, R. D. Walshaw, B. J. Murray, F. C. Meldrum, and H. K. Christenson, "High-speed imaging of ice nucleation in water proves the existence of active sites," Sci. Adv. **5**(2), 1–11 (2019).

[35] A. Kiselev, F. Bachmann, P. Pedevilla, S. J. Cox, A. Michaelides, D. Gerthsen, and T. Leisner, "Active sites in heterogeneous ice nucleation—The example of K-rich feldspars," Science **355**(6323), 367–371 (2017).

[36] F. K. Crundwell, "The mechanism of dissolution of minerals in acidic and alkaline solutions: Part IV equilibrium and near-equilibrium behaviour," Hydrometallurgy **153**, 46–57 (2015).

[37] A. Kumar, C. Marcolli, and T. Peter, "Ice nucleation activity of silicates and aluminosilicates in pure water and aqueous solutions – Part 3: Aluminosilicates," Atmos. Chem. Phys. **19**(9), 6059–6084 (2019).

[38] E. S. Chardon, F. R. Livens, and D. J. Vaughan, "Reactions of feldspar surfaces with aqueous solutions," Earth-Sci. Rev. **78**(1–2), 1–26 (2006).

[39] D. M. Murphy and D. S. Thomson, "Chemical composition of single aerosol particles at Idaho Hill: Positive ion measurements," J. Geophys. Res.: Atmos. **102**(D5), 6341–6352, https://doi.org/10.1029/96jd00858 (1997).

[40] E. Anim-Danso, Y. Zhang, and A. Dhinojwala, "Surface charge affects the structure of interfacial ice," J. Phys. Chem. C **120**(7), 3741–3748 (2016).

[41] G. Gonella, E. H. G. Backus, Y. Nagata, D. J. Bonthuis, P. Loche, A. Schlaich, R. R. Netz, A. Kühnle, I. T. McCrum, M. T. M. Koper, M. Wolf, B. Winter, G. Meijer, R. K. Campen, and M. Bonn, "Water at charged interfaces," Nat. Rev. Chem **5**(7), 466–485 (2021).

[42] A. Kumar, C. Marcolli, B. Luo, and T. Peter, "Enhanced ice nucleation efficiency of microcline immersed in dilute NH$_3$ and NH$_4^+$-containing solutions," Atmos. Chem. Phys. Discuss. (published online 2018).

[43] T. F. Whale, M. A. Holden, T. W. Wilson, D. O'Sullivan, and B. J. Murray, "The enhancement and suppression of immersion mode heterogeneous ice-nucleation by solutes," Chem. Sci. **9**(17), 4142–4151 (2018).

[44] L. Chen, S. E. Worthy, W. Gu, A. K. Bertram, and M. Tang, "The effects of aminium and ammonium cations on the ice nucleation activity of K-feldspar," J. Geophys. Res.: Atmos. **128**(24), e2023JD039971, https://doi.org/10.1029/2023JD039971 (2023).

[45] X. Wei, P. B. Miranda, C. Zhang, and Y. R. Shen, "Sum-frequency spectroscopic studies of ice interfaces," Phys. Rev. B **66**(8), 085401 (2002).

[46] K. Blow, T. F. Whale, D. Quigley, and G. C. Sosso, "Understanding the impact of ammonium ion substitutions on heterogeneous ice nucleation," Faraday Discuss. **249**, 114–132 (2024).

[47] T. F. Whale, "Disordering effect of the ammonium cation accounts for anomalous enhancement of heterogeneous ice nucleation," J. Chem. Phys. **156**(14), 144503 (2022).

[48] G. Franceschi, P. Kocán, A. Conti, S. Brandstetter, J. Balajka, I. Sokolović, M. Valtiner, F. Mittendorfer, M. Schmid, M. Setvín, and U. Diebold, "Resolving the intrinsic short-range ordering of K$^+$ ions on cleaved muscovite mica," Nat. Commun. **14**(1), 208 (2023).

[49] A. Kyono, M. Kimata, and T. Hatta, "Aluminum position in Rb-feldspar as determined by X-ray photoelectron spectroscopy," Naturwissenschaften **90**(9), 414–418 (2003).

[50] F. Huber and F. J. Giessibl, "Low noise current preamplifier for qPlus sensor deflection signal detection in atomic force microscopy at room and low temperatures," Rev. Sci. Instrum. **88**(7), 073702 (2017).

[51] B. Schulze Lammers, D. Yesilpinar, A. Timmer, Z. Hu, W. Ji, S. Amirjalayer, H. Fuchs, and H. Mönig, "Benchmarking atomically defined AFM tips for chemical-selective imaging," Nanoscale **13**(32), 13617–13623 (2021).

[52] S. Sadewasser and T. Glatzel, in *Kelvin Probe Force Microscopy*, *Springer Series in Surface Sciences*, edited by S. Sadewasser and T. Glatzel (Springer International Publishing, Cham, 2012), Vol. 48.

[53] G. Kresse and J. Hafner, "*Ab initio* molecular dynamics for liquid metals," Phys. Rev. B **47**(1), 558–561 (1993).

[54] G. Kresse and J. Furthmüller, "Efficiency of ab-initio total energy calculations for metals and semiconductors using a plane-wave basis set," Comput. Mater. Sci. **6**(1), 15–50 (1996).

[55] S. Ehlert, U. Huniar, J. Ning, J. W. Furness, J. Sun, A. D. Kaplan, J. P. Perdew, and J. G. Brandenburg, "r^{2}SCAN-D4: Dispersion corrected meta-generalized gradient approximation for general chemical applications," J. Chem. Phys. **154**(6), 061101 (2021).

[56] P. Hapala, G. Kichin, C. Wagner, F. S. Tautz, R. Temirov, and P. Jelínek, "Mechanism of high-resolution STM/AFM imaging with functionalized tips," Phys. Rev. B **90**(8), 085421 (2014).

[57] P. Hapala, R. Temirov, F. S. Tautz, and P. Jelínek, "Origin of high-resolution IETS-STM images of organic molecules with functionalized tips," Phys. Rev. Lett. **113**(22), 226101 (2014).

[58] L. Pérez Ramírez, J. J. Gallet, F. Bournel, F. Lim, S. Carniato, F. Rochet, O. V. Yazyev, A. Pasquarello, E. Magnano, and F. Bondino, "Hydrogen bonding of ammonia with (H,OH)-Si(001) revealed by experimental and ab initio photoelectron spectroscopy," J. Phys. Chem. A **124**(26), 5378–5388 (2020).

[59] H. Landmesser, H. Kosslick, W. Storek, and R. Fricke, "Interior surface hydroxyl groups in ordered mesoporous silicates," Solid State Ionics **103**, 271–277 (1997).

[60] C. Guimon, A. Gervasini, and A. Auroux, "XPS study of the adsorption of SO$_2$ and NH$_3$ over supported tin dioxide catalysts used in de-NO$_x$ catalytic reaction," J. Phys. Chem. B **105**(42), 10316–10325 (2001).